01 Mar 2010

Determination of Structure Parameters in Strong-Field Tunneling Ionization Theory of Molecules

Song-Feng Zhao

Cheng Jin

Anh-Thu Le
Missouri University of Science and Technology, lea@mst.edu

T. F. Jiang

et. al. For a complete list of authors, see https://scholarsmine.mst.edu/phys_facwork/1622

Recommended Citation

S. Zhao et al., "Determination of Structure Parameters in Strong-Field Tunneling Ionization Theory of Molecules," *Physical Review A - Atomic, Molecular, and Optical Physics*, vol. 81, no. 3, American Physical Society (APS), Mar 2010.
The definitive version is available at https://doi.org/10.1103/PhysRevA.81.033423

Determination of structure parameters in strong-field tunneling ionization theory of molecules

Song-Feng Zhao,[1,2] Cheng Jin,[1,2] Anh-Thu Le,[1] T. F. Jiang,[1,3] and C. D. Lin[1]

[1]*J. R. Macdonald Laboratory, Physics Department, Kansas State University, Manhattan, Kansas 66506-2604, USA*

[2]*College of Physics and Electronic Engineering, Northwest Normal University, Lanzhou, Gansu 730070, People's Republic of China*

[3]*Institute of Physics, National Chiao-Tung University, Hsinchu 30010 Taiwan*

(Received 21 January 2010; published 29 March 2010)

In the strong field molecular tunneling ionization theory of Tong *et al.* [Phys. Rev. A **66**, 033402 (2002)], the ionization rate depends on the asymptotic wave function of the molecular orbital from which the electron is removed. The orbital wave functions obtained from standard quantum chemistry packages in general are not good enough in the asymptotic region. Here we construct a one-electron model potential for several linear molecules using density functional theory. We show that the asymptotic wave function can be improved with an iteration method and after one iteration accurate asymptotic wave functions and structure parameters are determined. With the new parameters we examine the alignment-dependent tunneling ionization probabilities for several molecules and compare with other calculations and with recent measurements, including ionization from inner molecular orbitals.

DOI: 10.1103/PhysRevA.81.033423 PACS number(s): 33.80.Rv, 42.50.Hz

I. INTRODUCTION

Tunneling ionization of molecules in strong infrared fields is the first step in many interesting strong-field phenomena such as high-order harmonic generation (HHG), emission of high-energy above-threshold ionization (HATI) electrons, and nonsequential double ionization (NSDI). Essential understanding to these processes is the angle-dependent ionization probability $P(\theta)$ for a molecule fixed in space, where θ is the angle between the molecular axis and the polarization direction of the laser's electric field. Since molecules are generally not fixed in space, i.e., not at a fixed alignment and/or orientation, experimental determination of $P(\theta)$ from partially aligned molecules requires additional assumptions. Alnaser *et al.* [1] first determined $P(\theta)$ from NSDI processes where the alignment of the molecule is determined by Coulomb explosion of the molecular ions. $P(\theta)$ can also be determined by ionizing partially aligned molecules [2,3] or by measuring the angular distribution of electrons removed by a circularly polarized laser [4,5]. In both methods the alignment of the molecular axis is determined by Coulomb explosion when the molecular ion is further ionized by an intense circularly polarized laser. In all of these measurements, the $P(\theta)$ is not determined directly for a fixed angle and some approximations are used in order to determine the alignment-dependent ionization probability.

Theoretically, $P(\theta)$ can in principle be obtained directly from numerical solution of the time-dependent Schrödinger equation (TDSE). However, even for the simplest H_2^+, the $P(\theta)$ obtained from solving TDSE by different groups still exhibits relatively large differences. While calculations of $P(\theta)$ for interesting multielectron molecular systems have been carried out using the time-dependent density-functional theory (TDDFT) (see, for example, Ref. [6]), the accuracy of these calculations is difficult to evaluate. Furthermore, these calculations are rather time-consuming. Besides these *ab initio* approaches, alignment-dependent tunneling ionization rate for molecules can be calculated using simple models such as the molecular strong field approximation (SFA) [7,8] or the molecular tunneling ionization theory [9]. The latter is the simplest and is a generalization of the tunneling model of Ammosov, Delone, and Krainov (ADK) [10] for atoms. In the molecular tunneling ionization model (MO-ADK) of Tong *et al.* [9], the ionization rate for a molecule aligned at an angle θ with respect to the laser polarization axis is given analytically. The ionization rate depends on the instantaneous electric field of the laser, the ionization potential of the molecule. Since it is a tunneling model, MO-ADK theory also depends on some structure parameters that relate the electronic density of the highest occupied molecular orbital (HOMO) in the asymptotic region. Subsequent further extension of the MO-ADK theory can be found in Refs. [11–13].

In Tong *et al.* [9], the structure parameters are extracted from molecular wave functions calculated using the multiple scattering method [14]. However, these days molecular wave functions are more easily accessible from quantum chemistry packages such as GAMESS [15], GAUSSIAN [16], and others. These codes provide many options, including the density functional theory approach, for calculating all the occupied molecular orbitals, such as HOMO-1 and HOMO-2, i.e., the first and second occupied orbital below HOMO. Thus it is desirable to obtain structure parameters from the asymptotic behavior of orbitals calculated from such packages. This was carried out for CO_2 by Le *et al.* [17] and for other molecules by Kjeldsen and Madsen [18]. Unfortunately, molecular orbitals from these chemistry packages are calculated using Gaussian basis functions and they are not suitable for representing the exponential decay of the wave function at large distances. As more accurate experimental data are becoming available, it is essential to redetermine these structure parameters more accurately. Since the asymptotic wave function does not contribute much to the total energy of a molecule, one cannot efficiently improve the asymptotic wave functions by enlarging the size of the Gaussian basis directly.

In this article, we describe how to improve the asymptotic wave function where the structure parameters are extracted. Our input consists of wave functions of all the occupied orbitals obtained from GAMESS or GAUSSIAN. We then construct a single-active-electron model potential and solve the time-*in*dependent Schrödinger equation to obtain the molecular orbital wave functions by an iterative procedure. The details of

the method are given in Sec. II. We then apply the method to redetermine all the structure parameters previously published in Ref. [9] and add structure parameters for some inner orbitals. We also determine the structure parameters for a number of systems that have been investigated experimentally. Using these new structure parameters we examined the alignment dependence of ionization probabilities for several systems. In most cases, the new results do not differ much from what were presented in Tong *et al.* [9]. However, there are differences in some molecules. The strong deviation in CO_2 has been reported recently [19].

II. THEORETICAL METHODS

The theory part is divided into three subsections. We first present the method of generating a single-active-electron model potential for linear molecules. We then discuss how to calculate the wave functions by solving the time-*in*dependent Schrödinger equation with B-spline basis functions. We will also briefly describe how to extract the structure parameters in the MO-ADK theory.

A. Construction of single-active-electron model potentials for linear molecules

Single-active-electron model potential approach has been widely used for describing atoms in strong-field physics (see, for example, Ref. [20]). This approach has also been used for molecular targets recently [19,21]. The one-electron model potential consists of two parts: electrostatic and exchange-correlation terms. It is well known that the traditional local-density approximation (LDA) for the exchange-correlation potential does not give the correct $(-1/r)$ potential in the asymptotic region where the structure parameters are to be extracted. In this article, we follow Abu-samha and Madsen [21] and use the LB potential, proposed by Leeuwen and Baerends [22], which will give the correct asymptotic $-1/r$ behavior for neutral atoms and molecules. We note that a similar LB potential, called LBα [23], has also been used by Chu and collaborators in their TDDFT approach [6,24].

For linear molecules, the model potential can be expressed in single-center expansion as

$$V(r,\theta)=\sum_{l=0}^{l_{\max}} v_l(r)P_l(\cos\theta). \tag{1}$$

Here, v_l(r) is the radial component of the model potential and $P_l(\cos\theta)$ the Legendre polynomial. Typically we choose $l_{\max}=40$. The radial potential is given by

$$v_l(r)=v_l^{\rm nuc}(r)+v_l^{el}(r)+v_l^{ex}(r), \tag{2}$$

where the first two terms represent the electrostatic potential and the last term is the exchange interaction.

The electron-nucleus interaction $v_l^{\rm nuc}(r)$ can be written as

$$v_l^{\rm nuc}(r)=\sum_{i=1}^{N_a} v_l^i(r), \tag{3}$$

where i runs over the N_a atoms in the molecule. Without loss of generality, we assume that linear molecules are aligned along the z axis, then $v_l^i(r)$ can be expressed as

$$v_l^i(r)=\begin{cases} -\left(\frac{r_<^i}{r_>^i}\right)^l \frac{Z_c^i}{r_>^i} & \text{for } z_i>0 \\ -(-1)^l\left(\frac{r_<^i}{r_>^i}\right)^l \frac{Z_c^i}{r_>^i} & \text{for } z_i<0 \end{cases} \tag{4}$$

with $r_<^i=\min(r,|z_i|)$, $r_>^i=\max(r,|z_i|)$. Here Z_c^i and z_i are the nuclear charge and the z coordinate of the ith atom, respectively.

The partial Hartree potential $v_l^{el}(r)$ is given by

$$v_l^{el}(r)=\frac{4\pi}{2l+1}\int_0^\infty a_l(r')r'^2\frac{r_<^l}{r_>^{l+1}}dr' \tag{5}$$

with $r_<=\min(r,r')$, $r_>=\max(r,r')$. Here $a_l(r')$ is

$$a_l(r')=\frac{2l+1}{2}\int_{-1}^{1}\rho(r',\theta')P_l(\cos\theta')d(\cos\theta'), \tag{6}$$

where ρ is the total electron density in the molecule and

$$\rho(r',\theta')=\sum_{i=1}^{N_e}\frac{1}{2\pi}\int_0^{2\pi}|\Psi_i(r',\theta',\varphi')|^2d\varphi'. \tag{7}$$

Here i runs over all the N_e electrons in the molecule. The wave function of each molecular orbital can be obtained from quantum chemistry packages such as GAMESS [15] and GAUSSIAN [16].

For the partial exchange potential, it is written as

$$v_l^{ex}(r)=\frac{2l+1}{2}\int_{-1}^{1}V_{ex,\sigma}(r,\theta)P_l(\cos\theta)d(\cos\theta), \tag{8}$$

where

$$V_{ex,\sigma}(r,\theta)=\alpha V_{ex,\sigma}^{\rm LDA}(r,\theta)+V_{ex,\sigma}^{\rm GC}(r,\theta). \tag{9}$$

Here $V_{ex,\sigma}^{\rm LDA}(r,\theta)$ is the LDA potential for an electron with spin σ

$$V_{ex,\sigma}^{\rm LDA}(r,\theta)=-\left[\frac{6}{\pi}\rho_\sigma(r,\theta)\right]^{1/3}, \tag{10}$$

where

$$\rho_\sigma(r,\theta)=\sum_{i=1}^{N_\sigma}\frac{1}{2\pi}\int_0^{2\pi}|\Psi_{i\sigma}(r,\theta,\varphi)|^2d\varphi. \tag{11}$$

Here i runs over the N_σ electrons that have the same spin as the active electron. The gradient correction term is given by [22]

$$V_{ex,\sigma}^{\rm GC}(r,\theta)=-\frac{\beta\chi_\sigma^2(r,\theta)\rho_\sigma^{1/3}(r,\theta)}{1+3\beta\chi_\sigma(r,\theta)\sinh^{-1}(\chi_\sigma(r,\theta))}, \tag{12}$$

where $\chi_\sigma(r,\theta)=|\nabla\rho_\sigma(r,\theta)|\rho_\sigma^{-4/3}(r,\theta)$. The parameters α and β are chosen to be 1.0 and 0.05, respectively throughout this paper. We note that for more accurate binding energies, the correlation potential should be included into Eq. (9). In the so-called LBα model, the two parameters α and β are usually chosen to be 1.19 and 0.01, respectively (see Ref. [23]).

B. Calculation of molecular wave functions by solving the time-*in*dependent Schrödinger equation

With the model potential constructed in the previous subsection, the wave function for the active electron in a

linear molecule can be obtained by solving the following time-*in*dependent Schrödinger equation

$$H_{el}\psi_n^{(m)}(\boldsymbol{r}) \equiv \left[-\tfrac{1}{2}\nabla^2 + V(r,\theta)\right]\psi_n^{(m)}(\boldsymbol{r}) = E_n\psi_n^{(m)}(\boldsymbol{r}) \quad (13)$$

where $\psi_n^{(m)}$ and $E_n^{(m)}$ are the eigenfunction and eigenvalue, respectively.

Using single-center expansion for the electronic wave function

$$\psi_n^{(m)}(\boldsymbol{r}) = \sum_{l=0}^{l_{\max}} \frac{u_{nl}(r)}{r} Y_{lm}(\theta,\varphi), \quad (14)$$

where $Y_{lm}(\theta,\varphi)$ are the spherical harmonics, the radial wave function can be constructed with B-splines [25]

$$u_{nl}(r) = \sum_{i=1}^{N_l} c_{il}^n B_i(r). \quad (15)$$

Substituting Eqs. (1), (14), and (15) into Eq. (13) and then projecting onto the $B_i Y_{lm}^*$ basis, we obtain the following matrix equation

$$HC = ESC, \quad (16)$$

where

$$H_{il,i'l'} = \int_0^{r_{\max}}\int_0^{\pi}\int_0^{2\pi} B_i(r)Y_{lm}^*(\theta,\varphi)H_{el} \times B_{i'}Y_{l'm}(\theta,\varphi)dr\sin\theta d\theta d\varphi \quad (17)$$

$$S_{il,i'l'} = \delta_{ll'}\int_0^{r_{\max}} B_i(r)B_{i'}(r)dr \quad (18)$$

E and C are energy matrix and coefficient matrix, respectively. The eigenfunctions and eigenvalues are obtained by diagonalizing Eq. (16).

C. Extracting asymptotic structure parameters

In the asymptotic region, typically only a few terms in the single-center expansion Eq. (14) are important. Following Tong *et al.* [9], we write the wave function of a linear molecule as

$$\psi_n^{(m)}(\boldsymbol{r}) = \sum_l F_{lm}(r)Y_{lm}(\theta,\varphi). \quad (19)$$

In the MO-ADK theory [9], the radial functions in the asymptotic region are fitted to the following form

$$F_{lm}(r) = C_{lm}r^{(Z_c/\kappa)-1}e^{-\kappa r}, \quad (20)$$

where Z_c is the asymptotic charge and $\kappa = \sqrt{2I_p}$, I_p is the ionization energy.

III. RESULTS AND DISCUSSION

A. On the quality of the model potential and the iteration procedure

In this article, the single-active-electron model potential (see Sec. II A) is created with the DFT, in which the exchange potential is constructed with the exchange-only LDA potential and the LB model potential (or LDA + LB). First, we check the quality of this model potential if the molecular orbitals obtained from the standard quantum chemistry package GAMESS [15] are used as the input.

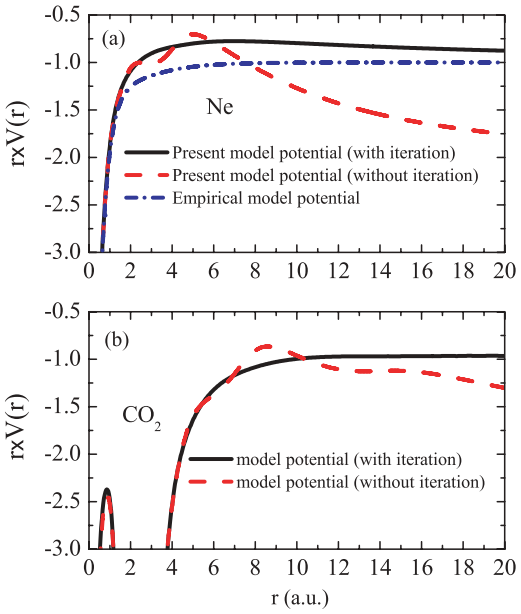

FIG. 1. (Color online) (a) Effective charge of Ne with and without the iteration (see text). Empirical model potential is from Ref. [20]. (b) Effective charge of CO_2 along the molecular axis.

In Fig. 1(a), we compare the present r-weighted model potential with the empirical model potential of Tong *et al.* [20] for Ne. For clarity we plot the effective charge, defined as $rV(r)$. The two potentials agree well in the small r region. However, there are significant differences at large r. For neutral atoms, the effective charge should approach -1 at large r. If the one-electron model potential is calculated directly using the molecular wave functions from GAMESS (dashed line) the effective charge exhibits oscillations and then drops rapidly with r. This undesirable behavior is due to the incorrect electron density, which in turn is due to the limitation of the Gaussian basis, calculated from GAMESS in the large r region. To correct this error, we perform one more iteration on the potential: First, an initial model potential is generated using the Hartree-Fock (HF) wave functions obtained from GAMESS. From this initial potential, more accurate wave functions are obtained by solving Eq. (13) with B-spline functions. Then, a new model potential is constructed from these new wave functions. From Fig. 1(a), we observe that the effective charge obtained after one iteration (solid line) shows the correct asymptotic behavior. The same procedure can be applied to molecules. In Fig. 1(b), we show the model potential of CO_2 along the molecular axis, with and without one iteration. It confirms that the asymptotic behavior of the model potential is correct after one iteration. We comment that in the case of CO_2 diffuse functions have been included in the basis sets. Clearly, this alone is insufficient for obtaining accurate electron density (or potential) at large r.

B. Extracting molecular structure parameters for the MO-ADK theory

Once the model potential is obtained, the eigenfunction and eigenvalue can be calculated from solving Eq. (13). In Table I, binding energies of rare gas atoms obtained using the

TABLE I. Comparison of calculated ionization energies of rare gas atoms in the exchange-only LDA + LB model and experimental values.

Atom	LDA + LB (a.u.)	I_p (a.u.)
He	0.786	0.904[a]
	0.796[b]	
Ne	0.722	0.793[a]
	0.725[b]	
Ar	0.524	0.579[a]
	0.528[b]	
Kr	0.499	0.515[a]
Xe	0.469	0.446[a]

[a]Reference [27].
[b]Reference [26].

present method are compared to those from Ref. [26] and the experimental values. Our method uses the same approximate exchange potential as in Ref. [26]. The two calculations agree in general, but discrepancies do exist with experimental values. This points out that the present one-electron model is still not sufficiently accurate for predicting the binding energy. The discrepancies can be reduced if correlation potential is included in Eq. (9). This fact has been well documented in Ref. [26]. As stated below, in MO-ADK theory, we always use experimental binding energy. If such information is not available, accurate binding energy can be calculated using MOLPRO [28].

In Table II, we compare the ionization energies from the present calculations with experimental vertical ionization energies for several linear molecules. The equilibrium distances of these molecules are also listed. The agreement between the calculated and experimental values are good. Again we comment that the exchange-only LDA + LB potential are used in our calculations. For higher precision, correlation potential should be included [6,23,24,29].

TABLE II. Equilibrium distances, ionization energies calculated in the exchange-only LDA + LB model and experimental vertical ionization potentials for several linear molecules.

Molecule	R (Å)	LDA + LB (eV)	I_p (eV)
H_2^+	1.058	29.99	29.99
D_2/H_2	0.742	13.65	15.47
N_2	1.098	14.99	15.58
O_2	1.208	10.62	12.03
F_2	1.412	16.03	15.70
S_2	1.889	10.36	9.36
CO	1.128	13.22	14.01
NO	1.151	9.14	9.26
SO	1.481	9.37	10.29
CO_2	1.163	14.63	13.78
C_2H_2	1.203 (R_{CC})	11.19	11.41
	1.058 (R_{CH})		
HF	0.917	15.03	15.77
HCl	1.275	11.41	12.75
HCN	1.067 (R_{CH})	13.46	13.80
	1.159 (R_{CN})		

TABLE III. The newly fitted C_{lm} coefficients vs. values from earlier references [9,17,30,31].

Molecule	C_{0m}	C_{1m}	C_{2m}	C_{3m}	C_{4m}	C_{5m}	C_{6m}	
$H_2^+(\sigma_g)$	4.52		0.62		0.03			
	4.37		0.05		0.00			[9]
$D_2/H_2(\sigma_g)$	1.78		0.11		0.00			
	2.51		0.06		0.00			[9]
	1.15		0.067		0.001			[30]
$N_2(\sigma_g)$	2.68		1.10		0.06			
	2.02		0.78		0.04			[9]
$O_2(\pi_g)$			0.52		0.03			
			0.62		0.03			[9]
$F_2(\pi_g)$			1.21		0.13			
			1.17		0.13			[9]
$S_2(\pi_g)$			1.37		0.17			
			0.81		0.07			[9]
$CO(\sigma)$	2.32	1.62	0.82	0.17	0.05			
	1.43	0.76	0.28	0.02	0.00			[9]
$NO(\pi)$		0.21	0.38	0.02	0.02			
		0.22	0.41	0.01	0.00			[9]
$SO(\pi)$		0.38	0.71	0.05	0.05			
		0.41	−0.31	0.01	0.00			[9]
$CO_2(\pi_g)$			1.97		0.40		0.04	
			2.88		1.71		0.43	[17]
$C_2H_2(\pi_u)$		1.16		0.18		0.02		
		1.14		0.27		0.04		[31]
$HF(\pi)$		0.88	0.03	0.02	0.01			
$HCl(\pi)$		1.23	0.01	0.05	0.01	0.01		
$HCN(\pi)$		1.50	0.09	0.24	0.02	0.02		

With the new wave functions, we reevaluate the structure parameters for a number of linear molecules. Table III lists the newly fitted C_{lm} coefficients with those listed in Tong *et al.* [9] and in others, if available. These parameters will be used to obtain the alignment-dependent tunneling ionization rates, following the MO-ADK theory [9].

C. Comparison of alignment-dependent ionization probabilities between MO-ADK and other calculations

Using the improved structure parameters tabulated in Table III, we now use the analytical formula in Tong *et al.* [9] to obtain alignment-dependent tunneling ionization probabilities for selected molecules that have also been carried out by other methods. The results are shown in Fig. 2. For simplicity, all the probabilities are normalized to 1.0 at the peak. First, we comment that for N_2, O_2, F_2 the normalized probabilities obtained using the new structure parameters do not show noticeable differences compared to the probabilities calculated using old structure parameters. From Table III, we note that the structure parameters for these three molecules do not change much. We emphasize that in calculating MO-ADK rates, one should always use the experimental vertical ionization energy since the tunneling ionization rate depends exponentially on the ionization potential. In Figs. 2(d) and 2(e), we notice that, interestingly, the MO-ADK results using the new C_{lm} give stronger angular dependence than the old ones for both H_2^+ and H_2. This is the result of the relatively larger C_{2m} as compared to C_{0m} in the present calculations. For H_2^+, the present result lies between the two calculations from solving TDSE. For

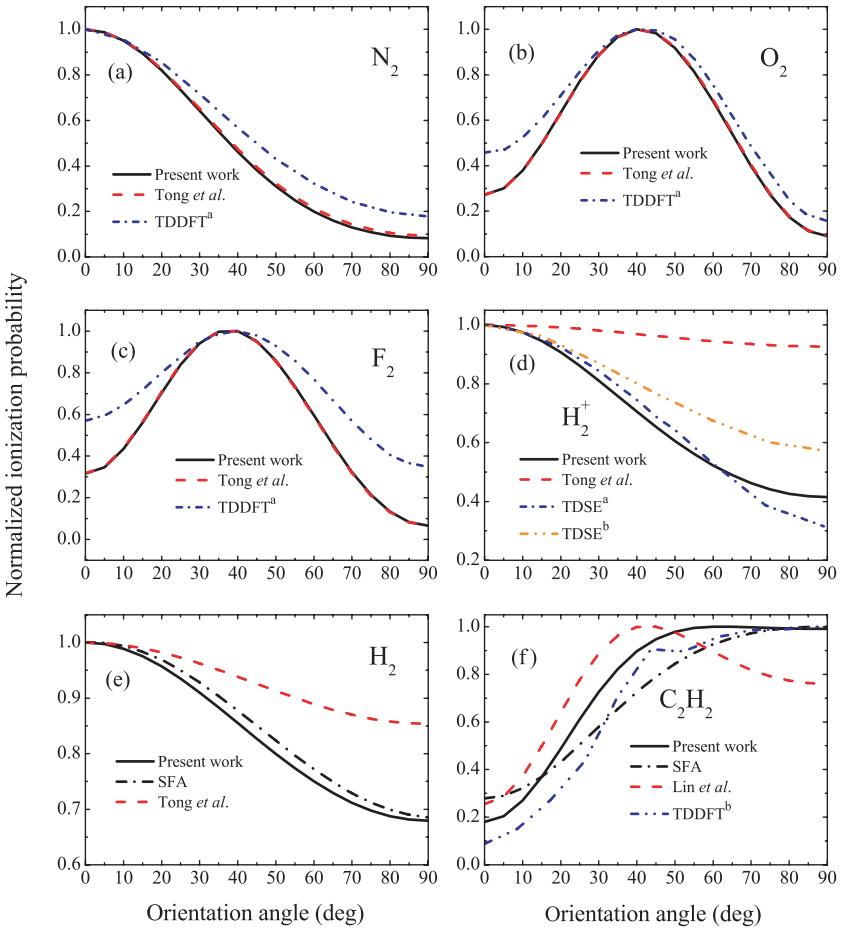

FIG. 2. (Color online) Normalized alignment dependence of ionization probability. (a) N_2 at laser intensity of 10^{14} W/cm^2; (b) O_2 at 10^{14} W/cm^2; (c) F_2 at 2×10^{14} W/cm^2; (d) H_2^+ at 5×10^{14} W/cm^2; (e) H_2 at 2.3×10^{14} W/cm^2; (f) C_2H_2 at 5×10^{13} W/cm^2. TDDFT^a from Telnov *et al.* [29], TDDFT^b from Otobe *et al.* [32], TDSE^a from Kamta *et al.* [33], TDSE^b from Kjeldsen *et al.* [34], Tong *et al.* [9], and Lin *et al.* [31].

H_2, we compare the new results with those from SFA, and the two agree quite well. For C_2H_2, the new MO-ADK result agrees with the SFA but differs from the older MO-ADK [31]. We comment that in the SFA calculation, wave functions directly from the GAMESS code are used. In general, SFA calculations yield incorrect total ionization rates. Empirically, however, the normalized alignment dependence from the SFA appears to be in agreement with the present MO-ADK. In presenting the SFA results, we always use the renormalized ones. We further comment that in SFA and other *ab initio* calculations, ionization probability or rate for each alignment angle is calculated independently. In the MO-ADK theory, the alignment dependence is obtained analytically after the structure parameters are obtained.

In recent years, *ab initio* calculations of molecular ionization by intense lasers have been carried out by solving the TDDFT [6,29,32]. These calculations include all the electrons in the molecule. Comparing to MO-ADK, in general, these calculations tend to give larger probabilities at angles where the ionization is small, see N_2 near 90° and O_2 and F_2 at angles near 0° and 90°. For C_2H_2, on the other hand, the TDDFT result is smaller at smaller angles than the present one. For this system, it was carried out by a different group [32]. Based on these results we can say that the alignment dependence of the ionization probabilities obtained from MO-ADK and from TDDFT are in reasonable agreement. However, we mention that probabilities in Fig. 2 from MO-ADK include ionization from the HOMO only, while the many-electron TDDFT calculations show significant contributions from the inner orbitals. More on the comparison between MO-ADK and TDDFT will be given later.

D. Alignment dependence of ionization rates from HOMO, HOMO-1, and HOMO-2 orbitals

Recently, strong field ionization phenomena involving inner orbitals of molecules have been reported widely [5,35–38]. This is somewhat surprising since tunneling ionization rate decreases very rapidly with the increase of ionization potential. However, molecular tunneling ionization rates depend on the symmetry of the orbital wave functions. For alignment angles where $P(\theta)$ is near the minimum for the HOMO but where HOMO-1 is near the maximum, there is a good possibility that ionization from HOMO-1 can become comparable or higher than from HOMO. Indeed, contribution from HOMO-1 to high-order harmonic generation (HHG) from N_2 molecules has been reported by McFarland *et al.* [35] when the molecules are aligned perpendicular to the polarization of the probe laser. Le *et al.* [36] have successfully reproduced the experimental results by including HHG from HOMO and HOMO-1. Since tunneling ionization is the first step for all rescattering processes [39–42], including HHG [41], it is pertinent to investigate P(θ) from inner orbitals as well.

In Table IV, the binding energies of HOMO, HOMO-1, and HOMO-2 for several molecules are shown. These energies are compared to calculations using the LBα model and

TABLE IV. Comparison of calculated binding energies of HOMO, HOMO-1, and HOMO-2 of N_2, O_2, and CO_2 in the present exchange-only LDA + LB model. Those from the LBα model and experimental vertical ionization potential are also given. Energies are in electron volts. For CO, HCl, and C_2H_2, only the energies of HOMO and HOMO-1 are considered.

Molecule	Spin orbital	LDA + LB	LBα	I_p
N_2	$3\sigma_g$(HOMO)	15.0	15.5[a]	15.6[b]
	$1\pi_u$(HOMO-1)	16.5	16.9[a]	17.2[b]
	$2\sigma_u$(HOMO-2)	17.8	18.5[a]	18.7[b]
O_2	$1\pi_g$(HOMO)	10.6	12.8[a]	12.3[c]
	$1\pi_u$(HOMO-1)	17.3	17.4[a]	16.7[c]
	$3\sigma_g$(HOMO-2)	17.1	18.3[a]	18.2[c]
CO_2	$1\pi_g$(HOMO)	14.6	13.9[d]	13.8[e]
	$1\pi_u$(HOMO-1)	18.3	17.5[d]	17.6[e]
	$3\sigma_u$(HOMO-2)	16.8	17.2[d]	18.1[e]
CO	5σ(HOMO)	13.2		14.0[e]
	1π(HOMO-1)	16.6		16.9[e]
HCl	2π(HOMO)	11.4		12.8[f]
	5σ(HOMO-1)	15.0		16.3[f]
C_2H_2	$1\pi_u$(HOMO)	11.2		11.4[e]
	$3\sigma_g$(HOMO-1)	15.7		16.4[e]

[a]Reference [29].
[b]Reference [43].
[c]Reference [44].
[d]Reference [6].
[e]Reference [45].
[f]Reference [46].

TABLE V. The C_l coefficients of HOMO, HOMO-1, and HOMO-2 for N_2, O_2, and CO_2 and of HOMO, HOMO-1, for CO, HCl, and C_2H_2. For σ orbital, $m = 0$ and π orbital, $m = 1$.

Molecule	Spin orbital	C_l				
N_2		C_{0m}	C_{2m}	C_{4m}		
	$3\sigma_g$(HOMO)	2.68	1.10	0.06		
		C_{1m}	C_{3m}	C_{5m}		
	$1\pi_u$(HOMO-1)	1.89	0.22	0.01		
	$2\sigma_u$(HOMO-2)	3.72	0.34	0.01		
O_2			C_{2m}	C_{4m}		
	$1\pi_g$(HOMO)		0.52	0.03		
		C_{1m}	C_{3m}	C_{5m}		
	$1\pi_u$(HOMO-1)	2.04	0.33	0.01		
		C_{0m}	C_{2m}	C_{4m}		
	$3\sigma_g$(HOMO-2)	3.05	1.59	0.08		
CO_2		C_{2m}	C_{4m}	C_{6m}		
	$1\pi_g$(HOMO)	1.97	0.40	0.04		
		C_{1m}	C_{3m}	C_{5m}	C_{7m}	
	$1\pi_u$(HOMO-1)	3.33	1.31	0.18	0.02	
	$3\sigma_u$(HOMO-2)	7.50	2.58	0.32	0.03	
CO		C_{0m}	C_{1m}	C_{2m}	C_{3m}	C_{4m}
	5σ(HOMO)	2.32	1.62	0.82	0.17	0.05
		C_{1m}	C_{2m}	C_{3m}	C_{4m}	C_{5m}
	1π(HOMO-1)	1.73	0.14	0.21	0.02	0.02
HCl		C_{1m}	C_{2m}	C_{3m}	C_{4m}	C_{5m}
	2π(HOMO)	1.23	0.01	0.05	0.01	0.01
		C_{0m}	C_{1m}	C_{2m}	C_{3m}	C_{4m}
	5σ(HOMO-1)	0.10	2.64	0.57	0.25	0.09
C_2H_2		C_{1m}	C_{3m}	C_{5m}		
	$1\pi_u$(HOMO)	1.16	0.18	0.02		
		C_{0m}	C_{2m}	C_{4m}	C_{6m}	
	$3\sigma_g$(HOMO-1)	4.40	3.85	0.72	0.09	

experimental values, to check the relative accuracy of the model we have used. We emphasize again that accurate experimental ionization energies, not the theoretical values in the table, are used in calculating the MO-ADK rates. The extracted C_{lm} parameters are given in Table V. Using these parameters and experimental ionization energies, the alignment dependence of ionization rates from different orbitals at a given peak laser intensity can be readily calculated.

In Fig. 3, we compare the ionization rates from N_2, O_2, and CO_2 molecules, for the HOMO, HOMO-1, and HOMO-2 orbitals, at peak intensities indicated in the figure. Note that the angular dependence, $P(\theta)$, reflects the shape of the molecular orbital quite accurately. Thus a σ orbital tends to have the peak at 0° and a minimum at 90°, a π_g orbital has the peak near 45° and minimum at 0° and 90°, and a π_u orbital has a peak near 90° and minimum near 0° [Deviations do occur, see the HOMO-1 of CO_2 in Fig. 3(c)]. These general behaviors of ionization rates explain why HOMO-2 is bigger than HOMO-1 at small angles for N_2, O_2, and CO_2, and why HOMO-1 is more important than HOMO at small angles for C_2H_2. Note that the relative ionization rates depend on laser intensities. The relative ionization rates for inner orbitals increases faster with increasing laser intensities. Using the parameters in Table V, their relative rates can be easily calculated using the MO-ADK model. We have also calculated the ionization rates using the molecular SFA. The relative alignment dependence from SFA in general agrees with those shown in Fig. 3. This is consistent with the findings in Le *et al.* [36].

Figure 4 shows the HOMO and HOMO-1 ionization rates for asymmetric diatomic molecules CO and HCl. There are recent experiments and other theoretical calculations available for these two molecules [5,37]. For both systems, the predictions from MO-ADK are also compared to results from SFA. Refer to Table IV, we note that the difference in binding energies between HOMO and HOMO-1 in CO is 2.9 eV and 3.5 eV for HCl. First we examine the θ dependence predicted by MO-ADK in Figs. 4(a) and 4(b). The HOMO of CO is a σ orbital; its $P(\theta)$ drops rapidly from 0° to 90° and stays relative flat at larger angles. The HOMO-1 is a π orbital and its $P(\theta)$ peaks near 90°. For HCl, the HOMO is a π orbital and it peaks near 90°. For the HOMO-1, it is a σ orbital and its P(θ) drops steadily till near 90°. Interestingly, its $P(\theta)$ increases rapidly from 90° to 180°, making it almost like a symmetric molecule.

Why are the σ orbitals of the two molecules so different? It is due to the degree of asymmetry in the wave functions. Such asymmetry is reflected in the C_l coefficients in Table V. For CO (HCl), the first three coefficients are 2.32, 1.62, 0.82 (0.10, 2.64, 0.57) for $l = 0$, 1 and 2, respectively. For HCl, there is one dominant $l = 1$ component only, thus the ionization rate is nearly symmetric. For CO, the two coefficients for $l = 0$ and 1 are comparable, the wave function along the axis for $\theta = 0$ and $\theta = \pi$ has the ratio $(2.32 + 1.62)/(2.32 - 1.62) = 5.6$. This gives a ionization rate ratio of 32, close to the value 50 read off from Fig. 4(a).

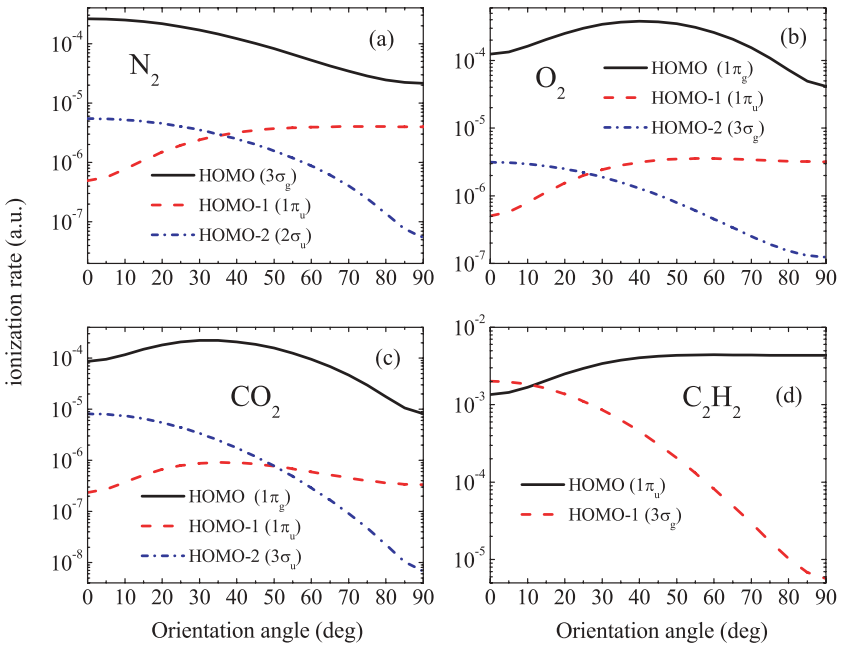

FIG. 3. (Color online) Alignment dependence of ionization rates of HOMO, HOMO-1, and HOMO-2 for N_2, O_2, and CO_2 and of HOMO and HOMO-1 for C_2H_2. (a) N_2 at laser intensity of 1.5×10^{14} W/cm^2; (b) O_2 at 1.3×10^{14} W/cm^2; (c) CO_2 at 1.1×10^{14} W/cm^2; (d) C_2H_2 at 1.5×10^{14} W/cm^2.

In Figs. 4(a) and 4(b), the θ dependence from SFA differs from that from MO-ADK. Recall that in MO-ADK, static ionization rate was calculated, thus a molecule is AB or BA with respect to the fixed electric field will have different rates. For a linearly polarized laser pulse, the direction of the electric field changes after each half cycle, thus the cycle-averaged rates for AB and BA are identical. To compare the SFA rate with the MO-ADK rate at an angle θ, we have to average the rates from the latter at θ and π-θ. These "symmetrized" ionization rates are denoted by MO-ADK-S in Fig. 4. By comparing the rates from SFA and MO-ADK-S, we found in Fig. 4(c) that the two models agree well for CO. For HCl, the relative rates for HOMO-1, normalized to HOMO, are about a factor of 2 larger from SFA than from MO-ADK. We comment that if ionization is measured using circularly polarized light, the static MO-ADK rate can be compared directly with the rate calculated using SFA.

The results of Figs. 3 and 4 show that at alignment angles where tunneling ionization from the HOMO is large, contributions from HOMO-1 or other inner orbitals are negligible. At alignment angles where HOMO is near the minimum, if the HOMO-1 (or even HOMO-2) is near the maximum, then these inner orbitals may become important. Since the relative tunneling ionization rates also depend on the peak laser intensity, when multiple orbitals contribute to strong field phenomena, the intensity dependence may become prominent. Experimentally, such multiple orbital effects, have been observed in HHG from N_2 when molecules are aligned

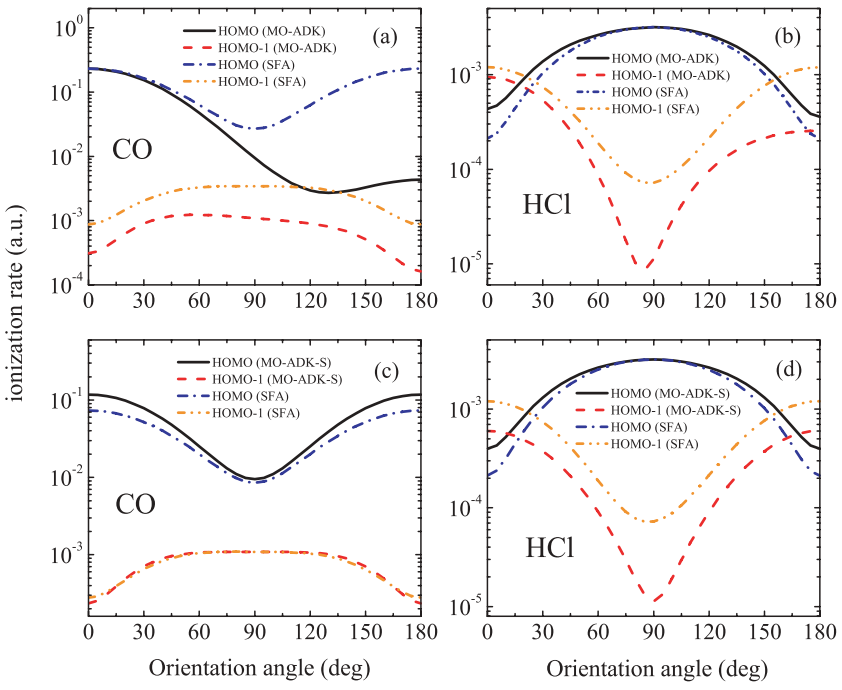

FIG. 4. (Color online) Alignment dependence of ionization rates of HOMO and HOMO-1. (a) CO at laser intensity of 4×10^{14} W/cm^2; (b) HCl at 2×10^{14} W/cm^2; (c) CO at 4×10^{14} W/cm^2; (d) HCl at 2×10^{14} W/cm^2. MO-ADK-S is the averaged MO-ADK rate for angles θ and $\pi - \theta$.

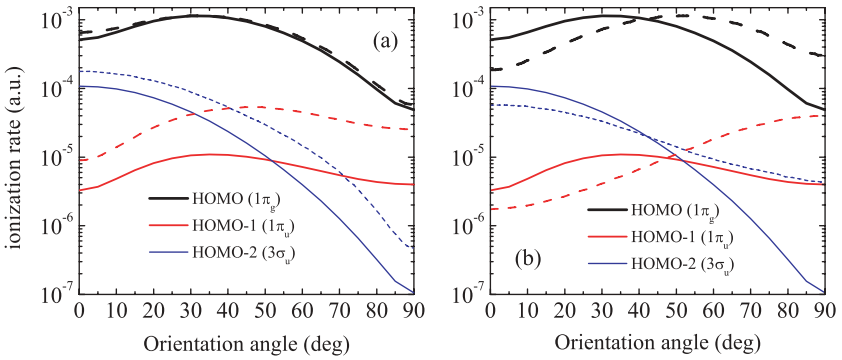

FIG. 5. (Color online) Comparison of ionization rates of HOMO, HOMO-1, and HOMO-2 of CO_2 at peak laser intensity of 1.5×10^{14} W/cm^2. The solid lines are from MO-ADK and the dashed lines are from Spanner and Patchkovskii [48] (a) and from Smirnova *et al.* [38] (b).

perpendicular to the laser's polarization axis [35,36]. The inner orbitals have been shown to become important in HHG from CO_2 when the molecules are aligned parallel to the laser's polarization axis [38]. Comparing to single photon ionization, strong field ionization tends to be more selective by ionizing the HOMO. For single-photon ionization, cross sections for HOMO, HOMO-1, and HOMO-2 in general have comparable values and often cross sections from inner orbitals are higher, see e.g., Ref. [47] for CO_2.

There are few theoretical alignment-dependent ionization rates from inner orbitals available to compare with the predictions of the MO-ADK theory presented here. There is an exception, however: CO_2. In Ref. [48] ionization rates from HOMO, HOMO-1, and HOMO-2 have been calculated starting from the multielectron perspective. In Fig. 5(a) we compare the rates from MO-ADK with those from Ref. [48] at the uncoupled channel approximation. The two sets of calculations are normalized at the peak of the HOMO curve. We note that the θ dependence agrees well for each orbital. For the HOMO, the agreement is "perfect." The rates for the inner orbitals are larger from Ref. [48] than from MO-ADK. Part of the reason of the larger difference in the HOMO-1 rate could be due to the difference in the ionization energy used. In Ref. [48], the energy difference between HOMO-1 and HOMO was taken to be 3.53 eV, while in MO-ADK, the difference was taken to be 3.80 eV from the experimental values in Table IV. For the HOMO-2 the energy used is the same for the two calculations. The alignment dependence of ionization rates for the three orbitals have also been calculated in Ref. [38] and the comparison with the present MO-ADK is given in Fig. 5(b), again by normalizing at the peak value of the HOMO. In this case the differences are larger. In Ref. [38], the ionization rates were calculated using Coulomb corrected SFA plus subcycle dynamics. The TDDFT method has also been used to obtain ionization probabilities from different orbitals [6,29]. For CO_2, the predicted alignment dependence for the HOMO, HOMO-1, and HOMO-2 as shown in Fig. 3 of Ref. [6] do agree with the present Fig. 3(c), including that the peak for HOMO-1 is not at 90°. However, we should comment that in N_2 and O_2, the alignment dependence using the same TDDFT method in Ref. [29] does not agree with Figs. 3(a) and 3(b) shown for these two molecules.

E. Comparisons with experiments

Figure 6 shows the normalized alignment dependence of ionization probability of N_2, O_2, H_2 and HCl. From Figs. 6(a) and 6(b), we comment that the normalized ionization

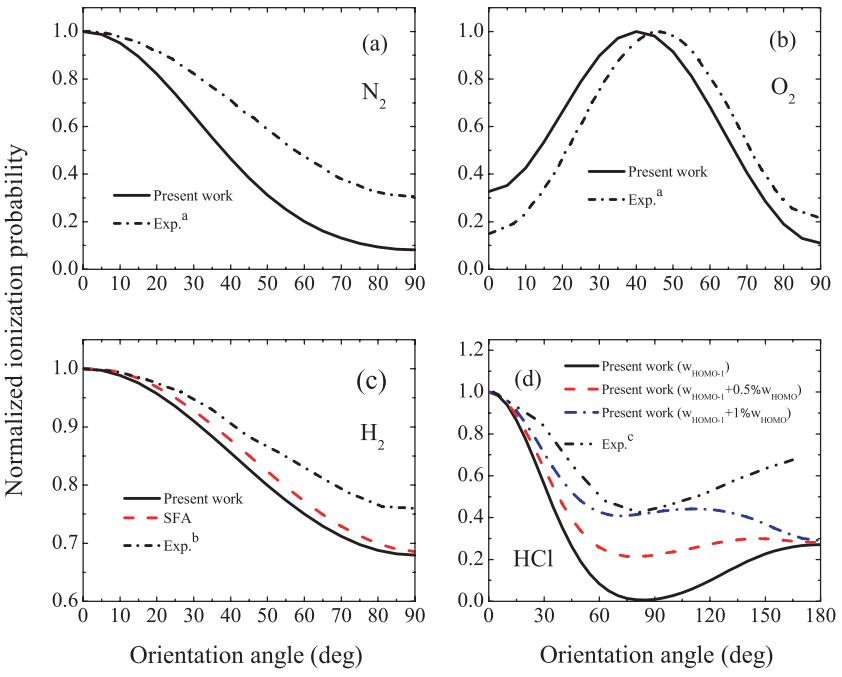

FIG. 6. (Color online) Normalized alignment dependence of ionization probability. (a) N_2 at laser intensity of 1.5×10^{14} W/cm^2; (b) O_2 at 1.3×10^{14} W/cm^2; (c) H_2 at 2.3×10^{14} W/cm^2; (d) HCl at 1.4×10^{14} W/cm^2. Linearly polarized lights for (a) and (b); circularly polarized lights for (c) and (d). Exp.^{a} from Pavičić *et al.* [3]; Exp.^{b} from Staudte *et al.* [4] and Exp.^{c} from Akagi *et al.* [5]. Additional symbols for (d), see text.

probability of N_2 calculated from MO-ADK theory using the old and the newly fitted coefficients agree quite well (no visible difference in the plot). Compared to the experiment of Pavičić *et al.* [3], the MO-ADK theory shows some differences. But the difference is considered acceptable. Note that the determination of alignment dependence from the experiment has angular average which was not included in the theory curve. Take the experimental result as reference, the TDDFT result (see Fig. 2) is better than the MO-ADK for N_2. For O_2, it is the other way around. The same comparison for CO_2 has been addressed in an earlier article [19]. In that case, the old MO-ADK results were found to be inaccurate due to the inaccuracy of the old C_l parameters. In Ref. [19] it was further concluded that the experimental $P(\theta)$ from Ref. [3] appears to be too narrowly peaked. We note that the new result from Ref. [48] also does not agree with that of the experiment. However, the authors suspect that the discrepancy is due to intermediate excitation channels that were not included in their calculation. We tend to think that additional experiments are needed to help resolving this discrepancy.

In Fig. 2(e) we show that the MO-ADK probabilities for H_2 using the new structure parameters differ from those using the earlier ones [9]. The new MO-ADK probabilities and molecular SFA agree well; see Fig. 6(c). Comparing to experimental data of Staudte *et al.* [4], the agreement is good in view that the theory curve has not included average over angular resolution. In Ref. [4], the ratio of ionization rate for molecules aligned parallel vs. perpendicular, with respect to the polarization axis, were also determined at four intensities from 2 to 4.5×10^{14} W/cm^2 (for circularly polarized laser). The ratio from the present SFA (not shown) agree with the SFA model in that article, and with the new MO-ADK ratio of 1.45 (the old MO-ADK gives 1.15). We expect the theoretical ratio be reduced somewhat if angular average is incorporated. We mention that a similar measurement at one intensity for laser wavelength of 1850 nm was reported in Ref. [49], which gives a ratio of 1.15. Interestingly, this ratio was reported to be 3.0 [50] in another recent experiment, while the theory presented in the same paper gives a ratio of 2.1. We comment that the ratio is taken at the maximum with respect to the minimum and thus sensitive to the angular average. Comparison of the rates over the whole angular range would be preferable.

In Fig. 6(d), the $P(\theta)$ of the HOMO-1 orbital in HCl reported in Ref. [5] using circularly polarized light at the intensity of 1.4×10^{14} W/cm^2 is shown. We compare the HOMO-1 result from the MO-ADK theory using the laser parameters given in the experiment and by normalizing the data at $\theta = 0^\circ$. In Ref. [5], the alignment dependence for HOMO and HOMO-1 has also been reported using the TDDFT. The alignment dependence between MO-ADK and TDDFT calculations are quite similar, but our relative HOMO-1 probability is about a factor of three higher at the same laser intensity. The ionization probability from both calculations drop much faster from 0° to 90° when compared to the experiment. By introducing a small fraction of the contribution from the HOMO in the manner suggested in Ref. [5], the MO-ADK theory can achieve a reasonable agreement with the experimental data from 0° to 90°, see Fig. 6(d). On the other hand, the agreement at angles larger than 90° is still not as good.

F. Ionization probability of H_2^+

The ionization probability of H_2^+ has been calculated from solving the TDSE by different groups [33,34,51]. It is of interest to compare the predictions based on MO-ADK with those from solving the TDSE. In Fig. 7, the normalized alignment-dependent ionization probability from the first four molecular orbitals of H_2^+ at the equilibrium distance are shown. The data for $1s\sigma_g$ have been discussed earlier [19]. For ionization from $1s\sigma_u$, the two TDSE calculations and the MO-ADK agree quite well. For $2p\pi_u$, the MO-ADK theory

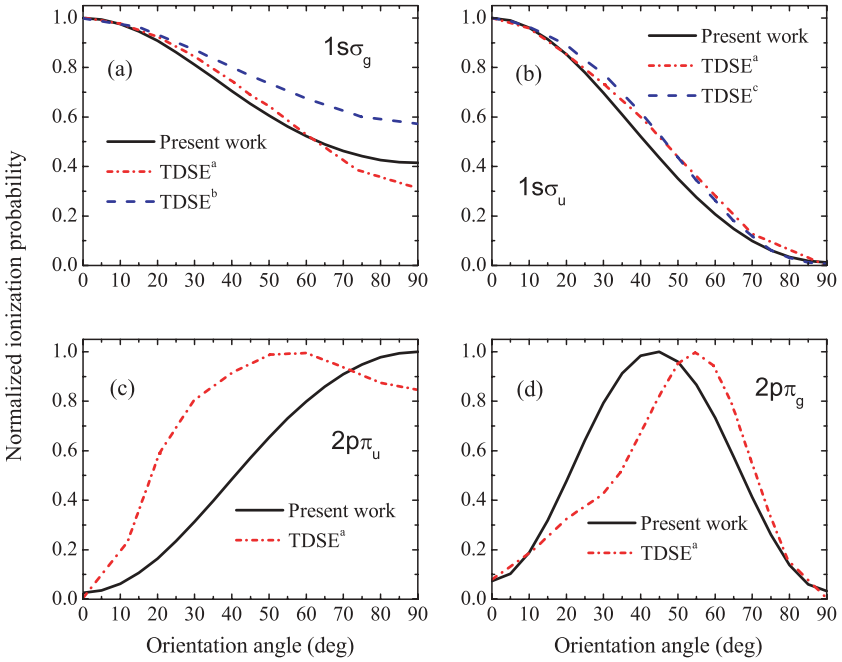

FIG. 7. (Color online) Normalized alignment dependence of ionization probability of H_2^+. (a) $1s\sigma_g$ at laser intensity of 5×10^{14} W/cm^2; (b) $1s\sigma_u$ at 10^{14} W/cm^2; (c) $2p\pi_u$ at 10^{13} W/cm^2; (d) $2p\pi_g$ at 10^{12} W/cm^2. TDSE^a from Kamta *et al.* [33], TDSE^b from Kjeldsen *et al.* [34] and TDSE^c from Telnov *et al.* [51].

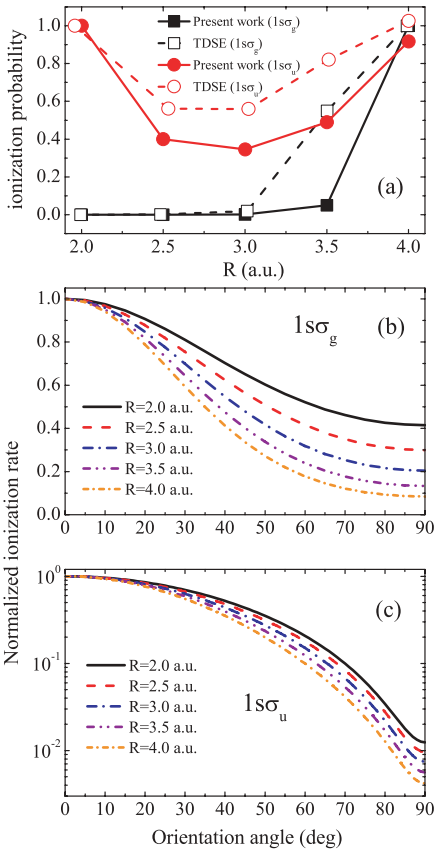

FIG. 8. (Color online) (a) R dependence of the normalized ionization probability of H_2^+ at laser intensity of $10^{14}\,W/cm^2$; see text. (b) The normalized alignment dependence of ionization rate at $5\times10^{14}\,W/cm^2$ for $1s\sigma_g$; (c) the normalized alignment dependence of ionization rate at $10^{14}\,W/cm^2$ for $1s\sigma_u$. TDSE from Ref. [52].

tends to peak at 90° while the TDSE result gives a peak closer to about 60°. For $2p\pi_g$ state, the MO-ADK predicts a peak near 45° while TDSE calculation gives a peak at about 55°. Note different peak laser intensities are used for the ionization from each orbital.

In Fig. 8(a) we show the dependence of normalized ionization probabilities vs the internuclear separation for the $1s\sigma_{g,u}$ states of H_2^+ with the molecular axis parallel to the polarization axis. The results are compared to the TDSE calculations of Ref. [52]. By normalizing the probability at $R=2$ a.u. for the $1s\sigma_u$, we find that there is a general good agreement between the TDSE result and from the MO-ADK. For the $1s\sigma_g$, the two calculations are normalized at $R=4.0$ a.u.. For both calculations, the probabilities at R less than 3.5 a.u. are significantly smaller than at $R=4.0$ a.u.. In Figs. 8(b) and 8(c), the normalized alignment-dependent ionization rates are shown for different R. Clearly as R increases, the angular dependence becomes sharper. This is easily understood for σ orbitals since the molecular orbital becomes more elongated along the molecular axis as R increases. The C_l coefficients are tabulated in Table VI to reflect how these parameters vary as R increases.

TABLE VI. The C_l coefficients of $1s\sigma_g$, $1s\sigma_u$, $2p\pi_g$, and $2p\pi_u$ for H_2^+ at different internuclear distances. For σ orbital, $m=0$ and π orbital, $m=1$. The calculated binding energies and exact ones (in atomic units) are also listed.

Symmetry	R (a.u.)	Binding energy		C_l		
$1s\sigma_g$		Present	Exact	C_{0m}	C_{2m}	C_{4m}
	2.0	1.1025	1.1026	4.52	0.62	0.03
	2.5	0.9937	0.9938	4.25	0.81	0.05
	3.0	0.9107	0.9109	4.10	1.04	0.08
	3.5	0.8463	0.8466	4.00	1.31	0.12
	4.0	0.7958	0.7961	3.96	1.60	0.19
$1s\sigma_u$				C_{1m}	C_{3m}	C_{5m}
	2.0	0.6674	0.6675	1.89	0.08	0.00
	2.5	0.6920	0.6921	2.18	0.15	0.00
	3.0	0.7012	0.7014	2.48	0.25	0.01
	3.5	0.7009	0.7012	2.79	0.37	0.02
	4.0	0.6952	0.6956	3.13	0.53	0.04
$2p\pi_g$					C_{2m}	C_{4m}
	2.0	0.4288	0.4288		0.11	0.002
$2p\pi_u$				C_{1m}	C_{3m}	
	2.0	0.2267	0.2267	0.90	0.02	

IV. CONCLUSIONS

In this article we proposed a method to obtain accurate molecular wave functions in the asymptotic region starting with molecular orbitals obtained from the widely used quantum chemistry packages such as GAMESS and GAUSSIAN. From these wave functions, the structure parameters in the molecular tunneling ionization theory (MO-ADK) of Tong *et al.* [9] can be accurately determined. Using these structure parameters, we reexamined the alignment-dependent tunneling ionization probabilities for a number of molecules, including ionization from HOMO-1 and HOMO-2 orbitals. The calculated tunneling ionization probabilities are compared to probabilities determined from experiments and to several other more elaborated calculations. Since tunneling ionization is the first step for strong field phenomena involving molecular targets, these structure parameters are useful and thus are tabulated. The procedure for obtaining the structure parameters discussed in this article is generally applicable to any linear molecules. Despite of its fundamental importance, accurate strong field alignment-dependent ionization probabilities are still not widely available. Experimental measurements as well as more advanced calculations tend to deal with different molecules and under different conditions, thus it is difficult to benchmark the accuracy of the theoretical models. While MO-ADK model is the simplest model for obtaining tunneling ionization rates, it appears that its predictions so far are in good agreement with most of the experimental data and with most the elaborate theoretical calculations.

ACKNOWLEDGMENTS

This work was supported in part by Chemical Sciences, Geosciences and Biosciences Division, Office of Basic Energy Sciences, Office of Science, US Department of Energy. S.-F.Z was also supported by the National Natural Science Foundation of China under Grant No. 10674112.

[1] A. S. Alnaser, S. Voss, X. M. Tong, C. M. Maharjan, P. Ranitovic, B. Ulrich, T. Osipov, B. Shan, Z. Chang, and C. L. Cocke, Phys. Rev. Lett. **93**, 113003 (2004).
[2] I. V. Litvinyuk, K. F. Lee, P. W. Dooley, D. M. Rayner, D. M. Villeneuve, and P. B. Corkum, Phys. Rev. Lett. **90**, 233003 (2003).
[3] D. Pavičić, K. F. Lee, D. M. Rayner, P. B. Corkum, and D. M. Villeneuve, Phys. Rev. Lett. **98**, 243001 (2007).
[4] A. Staudte, S. Patchkovskii, D. Pavičić, H. Akagi, O. Smirnova, D. Zeidler, M. Meckel, D. M. Villeneuve, R. Dörner, M. Yu. Ivanov, and P. B. Corkum, Phys. Rev. Lett. **102**, 033004 (2009).
[5] H. Akagi, T. Otobe, A. Staudte, A. Shiner, F. Turner, R. Dörner, D. M. Villeneuve, and P. B. Corkum, Science **325**, 1364 (2009).
[6] S. K. Son and Shih I. Chu, Phys. Rev. A **80**, 011403(R) (2009).
[7] J. Muth-Böhm, A. Becker, and F. H. M. Faisal, Phys. Rev. Lett. **85**, 2280 (2000).
[8] T. K. Kjeldsen and L. B. Madsen, J. Phys. B **37**, 2033 (2004).
[9] X. M. Tong, Z. X. Zhao, and C. D. Lin, Phys. Rev. A **66**, 033402 (2002).
[10] M. V. Ammosov, N. B. Delone, and V. P. Krainov, Zh. Eksp. Teor. Fiz. **91**, 2008 (1986) [Sov. Phys. JETP **64**, 1191 (1986)].
[11] Z. X. Zhao and T. Brabec, J. Phys. B **39**, L345 (2006).
[12] T. Brabec, M. Côté, P. Boulanger, and L. Ramunno, Phys. Rev. Lett. **95**, 073001 (2005).
[13] I. I. Fabrikant and G. A. Gallup, Phys. Rev. A **79**, 013406 (2009).
[14] D. Dill and J. L. Dehmer, J. Chem. Phys. **61**, 692 (1974).
[15] M. W. Schmidt *et al.*, J. Comput. Chem. **14**, 1347 (1993).
[16] M. J. Frisch *et al.*, GAUSSIAN *03, Revision C.02* (Gaussian Inc. Pittsburgh, PA, 2003).
[17] A.-T. Le, X. M. Tong, and C. D. Lin, J. Mod. Opt. **54**, 967 (2007).
[18] T. K. Kjeldsen and L. B. Madsen, Phys. Rev. A **71**, 023411 (2005).
[19] S.-F. Zhao, C. Jin, A.-T. Le. T. F. Jiang, and C. D. Lin, Phys. Rev. A **80**, 051402(R) (2009).
[20] X. M. Tong and C. D. Lin, J. Phys. B **38**, 2593 (2005).
[21] M. Abu-samha and L. B. Madsen, Phys. Rev. A **80**, 023401 (2009).
[22] R. van Leeuwen and E. J. Baerends, Phys. Rev. A **49**, 2421 (1994).
[23] P. R. T. Schipper, O. V. Gritsenko, S. J. A. van Gisbergen, and E. J. Baerends, J. Chem. Phys. **112**, 1344 (2000).
[24] Shih I. Chu, J. Chem. Phys. **123**, 062207 (2005).
[25] H. Bachau, E. Cormier, P. Decleva, J. E. Hansen, and F. Martín, Rep. Prog. Phys. **64**, 1815 (2001).
[26] A. Banerjee and M. K. Harbola, Phys. Rev. A **60**, 3599 (1999).
[27] J. Emsley, *The Elements* (Clarendon Press, Oxford, 1998).
[28] H.-J. Werner *et al.*, MOLPRO, *Version 2002.6, A Package of Ab Initio Programs* (Birmingham, UK, 2003).
[29] D. A. Telnov and Shih I. Chu, Phys. Rev. A **79**, 041401(R) (2009).
[30] M. Awasthi, Y. V. Vanne, A. Saenz, A. Castro, and P. Decleva, Phys. Rev. A **77**, 063403 (2008).
[31] C. D. Lin, X. M. Tong, and Z. X. Zhao, J. Mod. Opt. **53**, 21 (2006).
[32] T. Otobe and K. Yabana, Phys. Rev. A **75**, 062507 (2007).
[33] G. Lagmago Kamta and A. D. Bandrauk, Phys. Rev. A **74**, 033415 (2006).
[34] T. K. Kjeldsen, L. A. A. Nikolopoulos, and L. B. Madsen, Phys. Rev. A **75**, 063427 (2007).
[35] B. K. McFarland, J. P. Farrell, P. H. Bucksbaum, and M. Gühr, Science **322**, 1232 (2008).
[36] A.-T. Le, R. R. Lucchese, and C. D. Lin, J. Phys. B **42**, 211001 (2009).
[37] I. Znakovskaya, P. von den Hoff, S. Zherebtsov, A. Wirth, O. Herrwerth, M. J. J. Vrakking, R. de Vivie-Riedle, and M. F. Kling, Phys. Rev. Lett. **103**, 103002 (2009).
[38] O. Smirnova *et al.*, Nature (London) **460**, 972 (2009).
[39] T. Morishita, A.-T. Le, Z. Chen, and C. D. Lin, Phys. Rev. Lett. **100**, 013903 (2008).
[40] Z. Chen, A.-T. Le, T. Morishita, and C. D. Lin, Phys. Rev. A **79**, 033409 (2009).
[41] A.-T. Le, R. R. Lucchese, S. Tonzani, T. Morishita, and C. D. Lin, Phys. Rev. A **80**, 013401 (2009).
[42] S. Micheau, Z. Chen, A.-T. Le, and C. D. Lin, Phys. Rev. A **79**, 013417 (2009).
[43] A. Lofthus and P. H. Krupenie, J. Phys. Chem. Ref. Data **6**, 113 (1977).
[44] P. Baltzer, B. Wannberg, L. Karlsson, M. Carlsson Göthe, and M. Larsson, Phys. Rev. A **45**, 4374 (1992).
[45] D. W. Turner *et al.*, *Molecular Photoelectron Spectroscopy* (Wiley Interscience, London, 1970).
[46] P. Natalis, P. Pennetreau, L. Longton, and J. E. Collin, J. Electron Spectrosc. Relat. Phenom. **27**, 267 (1982).
[47] R. R. Lucchese and V. McKoy, Phys. Rev. A **26**, 1406 (1982).
[48] M. Spanner and S. Patchkovskii, Phys. Rev. A **80**, 063411 (2009).
[49] M. Magrakvelidze, F. He, S. De, I. Bocharova, D. Ray, U. Thumm, and I. V. Litvinyuk, Phys. Rev. A **79**, 033408 (2009).
[50] P. von den Hoff, I. Znakovskaya, S. Zherebtsov, M. F. Kling, and R. de Vivie-Riedle, Appl. Phys. B: Lasers Opt. (online available).
[51] D. A. Telnov and Shih I. Chu, Phys. Rev. A **76**, 043412 (2007).
[52] G. Lagmago Kamta and A. D. Bandrauk, Phys. Rev. A **75**, 041401(R) (2007).